Enhanced satellite remote sensing of coastal waters using spatially improved bio-optical products from SNPP–VIIRS

Ryan A. Vandermeulen [a,*], Robert Arnone [a], Sherwin Ladner [b], Paul Martinolich [c]

[a] University of Southern Mississippi, Department of Marine Science, Stennis Space Center, MS 39529, United States
[b] Naval Research Laboratory, Stennis Space Center, MS 39529, United States
[c] Vencore Incorporated, Stennis Space Center, MS 39529, United States

ARTICLE INFO

ABSTRACT

The spatial dynamics of coastal and inland regions are highly variable and monitoring these waters with ocean color remote sensors requires increased spatial resolution capabilities. A procedure for the spatial enhancement of ocean color products, including chlorophyll and inherent optical properties (IOPs), is developed using a sharpened visible water-leaving radiance spectrum for the visible infrared imaging radiometer suite (VIIRS). A new approach for spectral sharpening is developed by utilizing the spatial covariance of the spectral bands for sharpening the M bands (412, 443, 486, 551, 671 nm; 750-m resolution) with the I-1 band (645 nm; 375-m resolution). The spectral shape remains consistent by the use of a dynamic, wavelength-specific spatial resolution ratio that is weighted as a function of the relationship between proximate I- and M-band variance at each pixel. A comparison of bio-optical satellite products at 375-m and 750-m spatial resolution with in situ measurements of water leaving radiance and bio-optical properties show an improved capability of the VIIRS 375-m products in turbid and optically complex waters, such as the Chesapeake Bay and Mississippi River Plume. We demonstrate that the increased spatial resolution improves the ability for VIIRS to characterize bio-optical properties in coastal waters.

© 2015 Elsevier Inc. All rights reserved.

1. Introduction

Characterizing the dynamics of coastal optical water properties is a challenge due to the high spatial and temporal variability of optically active water constituents. These constituents include phytoplankton cells, suspended particulate material (SPM; both inorganic and organic), and chromophoric dissolved organic matter (CDOM), each of which have distinct optical signatures that affect the absorption and scattering of light in water, defining the water's inherent optical properties (IOPs; Kirk, 1992). Numerous coastal processes can drive the spatial distribution of optical water properties, such as fluvial input, tidal activity, eddy circulation, upwelling, and wind-driven mixing, thereby increasing the optical variability of these waters at scales of micrometers to kilometers (Dickey, 1991). As a result, major spatial limitations exist when attempting to characterize these complex waters with a shipboard sampling regime (Hu et al., 2004a; Miller, Twardowski, Moore, & Casagrande, 2003).

The spatial extent of these surface bio-optical properties can be determined from changes in satellite-detected water leaving radiance (L_w), enabling a more synoptic, albeit two-dimensional view of various ocean parameters on a global basis (Lewis, 1992). When using remote measurements to resolve ocean processes, two things must be considered: 1) the resolution capabilities of the remote detector, and 2) the spatial coherence of the process(es) to be studied. Spatial coherence describes the scales of variability within a system and helps determine the optimal pixel size for a satellite detector, or the ground sampling distance, to fully characterize the variability of a system. Semi-variogram analyses have shown that these spatial coherence scales are smaller in coastal and shelf waters and increase to larger scales in open ocean waters. Previous studies suggest a minimum ground sampling distance of 100-m for turbid estuaries (Bissett et al., 2004), while dominant scales of patchiness typical of coastal waters are resolved at 300 to 500-m spatial scales (Aurin, Mannino, & Franz, 2013; Davis, Kavanaugh, Letelier, Bissett, & Kohler, 2007).

The spatial resolution of many polar-orbiting sensors (~1 km) is often too coarse to fully unravel the variability associated with fine-scale coastal processes (IOCCG, 2012). Some sensors, such as the moderate/medium resolution imaging spectroradiometers (MODIS and MERIS, respectively) are equipped with higher spatial resolution bands (250–300 m), which have been successfully used to monitor

* Corresponding author at: University of Southern Mississippi, Department of Marine Science, 1020 Balch Blvd., Stennis Space Center, MS 39529, United States. Tel.: +1 228 688 7127.

E-mail address: Ryan.Vandermeulen@usm.edu (R.A. Vandermeulen).

coastal and inland waters for various parameters such as suspended solids (Miller & McKee, 2004), cyanobacterial blooms (Matthews, Bernard, & Winter, 2010), chlorophyll-a (Giardino, Candiani, & Zilioli, 2005; Moses, Gitelson, Berdnikov, & Povazhnyy, 2009), IOPs (Ladner et al., 2007), and general water quality (Floricioiu, Rott, Rott, Dokulil, & Defrancesco, 2004; Hu, Nababan, Biggs, & Muller-Karger, 2004b). While satellite systems with even higher spatial resolution capabilities do exist, such as the Hyperspectral Imager for the Coastal Ocean (HICO; 100-m spatial resolution), the Landsat series (30-m spatial resolution), or WorldView-2 (3-m spatial resolution), the temporal revisit time (1 + week) is not sufficient to resolve the temporal variability of coastal processes. These optically complex waters require the use of satellite sensors with sub-kilometer spatial resolution at all visible bands as well as a revisit time of at least once per day to capture the rapidly changing dynamics of coastal waters (Matthews, 2011).

The Suomi National Polar-orbiting Partnership (SNPP) satellite with the Visual Infrared Imaging Radiometer Suite (VIIRS) offers daily coverage of the world, with some limited regional coverage of more than once per day (Arnone et al., 2013). VIIRS has 7 visible/near infrared moderate resolution (M)-bands (λ = 410, 443, 486, 551, 671, 745, 865 nm) at a spatial resolution of 750-m at nadir, and two visible/near infrared imaging (I)-bands (λ = 640, 865 nm) at a spatial resolution of 375-m at nadir (Fig. 1). The 750-m bands offer spatial improvement compared to the analogous 1-km MODIS bands at nadir, in conjunction with a unique along-scan aggregation scheme that enables the retrieval of higher resolution data retrievals at high zenith angles (Baker, 2011). The utilization of the visible 375-m I1 band enables great potential to resolve the spatial variability present in complex coastal waters as the spatial scale offers four times more data than 750-m resolution M-bands, and approximately seven times more data than 1-km scales.

The higher resolution of the broad spectral I1 band (600–680 nm) may be used to spectrally enhance the spatial variability at other (lower resolution) visible wavelengths. In a previous study, Gumley, Descloitres, and Schmaltz (2010) used the 250-m high resolution MODIS band 1 (with similar spectral characteristics to VIIRS I1 band) to sharpen 500-m moderate resolution MODIS bands in order to produce true color imagery at a spatial resolution of 250-m. The Gumley et al. computation for MODIS sharpening is given as a ratio of high to low resolution top of the atmosphere (TOA) radiances:

$$R = \frac{B_{640}}{B_{640}^*} \tag{1}$$

where

R	spatial resolution ratio
B_{640}	band 1 (640 nm) at 250-m resolution
B_{640}^*	band 1 (640 nm) at 500-m resolution, projected to 250-m resolution (duplicated pixels)

The lower resolution spectral bands (in this case, the 500-m spatial resolution bands centered at λ = 470 and 555 nm) are subsequently sharpened by:

$$B_\lambda = RB_\lambda^* \tag{2}$$

where

B_λ	band (λ) at 250-m resolution
B_λ^*	band (λ) at 500-m resolution, interpolated to 250-m resolution

In short, the "spatial resolution ratio" empirically determines how each high resolution (MODIS band 1) pixel spatially differs from its neighboring pixel and applies that information about Band 1 variability to sharpen the lower resolution bands at other wavelengths. This sharpening technique works well for producing enhanced true color imagery, but it has the potential to introduce some spectral artifacts and cannot be applied to retrieve quantitative L_w measurements directly, as it centrally relies on the assumption that ocean color variability is unchanging across the visible spectrum. In other words, the approach assumes that the same spatial resolution differences that exist at 250-m in the red portion of the spectrum (645 nm) are also the same for the green and blue portions of the spectrum (410–555 nm). However, each optically active constituent in natural waters imparts its own unique spectral signature based on differing absorption and scattering coefficients, as well as its relative abundance. For example, high concentrations of suspended particles close to shore increase the backscattering coefficient relative to the absorption coefficient, which will be amplified in the red regions of the spectrum (600–700 nm) where there is lower absorption by particles (Miller & McKee, 2004). Meanwhile, wavelengths in the blue region of the spectrum, while also backscattered in the presence of suspended particles, are heavily influenced by absorption of phytoplankton cells, CDOM, and detrital material (Kirk, 1994). Therefore, what bio-optical variation is present in the red band (I1) is not strictly translatable to the bio-optical variability in the other visible bands.

Nevertheless, for spatially dynamic waters, such as those found in coastal regions, the high resolution I1 band can potentially yield useful information about ocean color variability. But in order to apply a spatial resolution ratio approach to sharpen other spectral bands, one must account for the dependence of spatial variability on spectral wavelength in waters of differing composition. In order to fully maximize the use of the VIIRS I1 band, we propose an adaptive image sampling technique that utilizes the relative covariance or divergence in radiance patterns occurring across the visible range of the light spectrum to spatially sharpen the visible spectral M(λ) bands. The objectives of this paper are to 1) demonstrate an enhanced spatial resolution in VIIRS by applying a spectrally weighted band-sharpening based on spatial coherence,
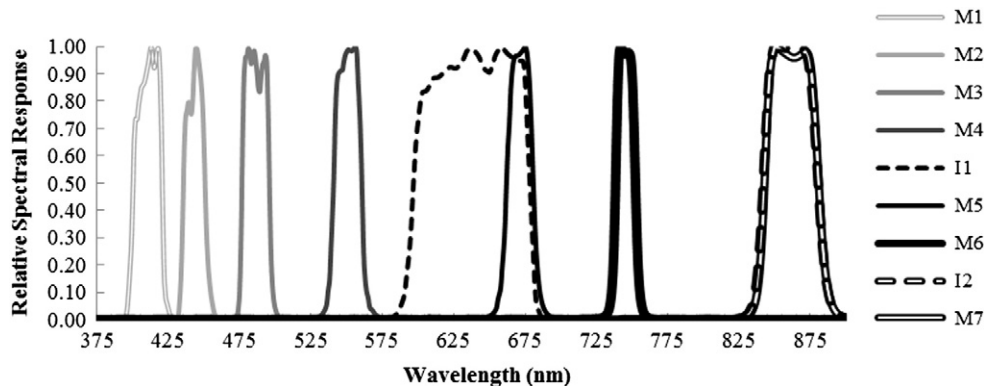

Fig. 1. The relative spectral response of the SNPP–VIIRS ocean color/NIR bands. Bands M1–M7 are at a resolution of 750-m, while the I1 and I2 bands have a higher spatial resolution (375-m).

2) ensure that optical consistency is maintained across the visible spectrum through qualitative and quantitative validation of the high resolution satellite products, and 3) demonstrate that increased resolution of bio-optical products improves the VIIRS characterization of coastal waters.

2. Data and methods

2.1. Initial satellite data processing

Level 1 VIIRS sensor data records (SDRs) were downloaded from NOAA's Comprehensive Large Array-data Stewardship System (CLASS, www.class.noaa.gov). All files were processed from SDRs (raw radiance + calibration) to environmental data records (EDRs; geophysical parameters) using the Naval Research Laboratory's Automated Processing System (APS v5.1). The APS uses the software package, n2gen, which is very similar to the open source l2gen software used by the NASA Ocean Biology Processing Group (OBPG). The APS is presently capable of processing the M bands of VIIRS to produce 750-m resolution bio-optical products, and also has the capability to process the five imaging bands. The scenes were processed using standard (Gordon & Wang, 1994) atmospheric correction at a resolution of 750-m, utilizing multi-scattering and iterative near infrared (NIR) correction (Stumpf, Arnone, Gould, Martinolich, & Ransibrahamanakul, 2003). Standard flags were used to mask interference from land, clouds, sun glint, and other potential disturbances to the radiance signal.

The proposed adaptive sharpening technique is a post-processing step that was performed on the atmospherically corrected normalized water leaving radiance (nLw) products using interactive data language (IDL). Normalized water leaving radiance is defined as the radiance backscattered out of the water in the absence of atmosphere and with the sun at the zenith (Gordon & Clark, 1981). The spectral nLw products are frequently used to compare satellite radiometry with in situ values, and are the basis for which subsequent bio-optical algorithms are calculated. It is important to perform the proposed sharpening function on nLw products to ensure that the derived spatial variability information is that associated with ocean color, and not the atmospheric components that are incorporated into the top of the atmosphere signal. In addition, the NIR iterative technique used in atmospheric correction algorithms is compromised when the resolution of the atmospheric correction bands differ from the visible bands. Attempts to sharpen the atmospheric correction with the I2 band (865 nm) were unsuccessful due to the low signal to noise (SNR) ratio of the I2 band compared to the M7 band (862 nm; Vandermeulen, Arnone, Ladner, & Martinolich, 2013).

2.2. Adaptive-sharpening technique

This new approach expands on the methodology described by Gumley et al. (2010), with some modifications. We will compute a similar spatial resolution ratio (Eq. 1) using the VIIRS I1 band to sharpen the VIIRS M(λ) bands, using atmospherically corrected nLw. In order to address the spectral dependence of optical variability in natural waters, we apply an adaptive weighting function to compute a wavelength dependent spatial resolution ratio. This ratio is based on the proximal covariance between the 375-m I1 band and each individual 750-m M(λ) band. The spectral 'weight' of the I1 band sharpening is determined at every wavelength from a spatial covariance ratio, $\rho(\lambda)$, and is computed from a moving 5×5 array surrounding each pixel in the image:

$$\rho(\lambda)_{\text{thresh}=1} = \frac{[\sigma/\mu]_{M(\lambda)}}{[\sigma/\mu]_{I1}} \qquad (3)$$

where

thresh = 1 Covariance ratio threshold; $\rho(\lambda)$ data greater than 1 converted to value of 1

$[\sigma/\mu]_{M(\lambda)}$ VIIRS M(λ) band coefficient of variance for 5×5 sub-array (M-band interpolated to 375-m)
$[\sigma/\mu]_{I1}$ VIIRS I1 band coefficient of variance for 5×5 sub-array

The covariance ratio, $\rho(\lambda)$, is obtained by dividing the M(λ) band coefficient of variance (standard deviation [σ]/mean [μ] of 5×5 sub-array surrounding the pixel) by the I band coefficient of variance of nLw at the same location. The M band is bi-linearly interpolated to 375-m projection in order to make statistical calculations comparable to that of the I1 band. In addition, all $\rho(\lambda)$ values > 1 are replaced with a value of 1 to prevent over sharpening in coastal regions. To clarify this action, since the denominator (I1 band) is not interpolated and represents true geophysical variability, we limit the influence of the weighting function based on the variability we confidently know exists, or, that within the I1 band, and not that which may have been interpolated by the M(λ) band.

The calculation of covariance between the I1 band and the M(λ) band ultimately enables the spatial resolution ratio to be optimized for each M(λ) band. Essentially, where the variability between the I1 band and a particular M(λ) band is similar at 750-m resolution, the assumption is made that there is similar spatial coherence at 375-m resolution as well. If this variability is resolved at each pixel, it is now possible to independently weight the spatial resolution ratio according to the relative variability present at each M(λ) band. The weight applied will change not only as a function of wavelength, but also the water type (i.e. high/low absorption/scattering waters), and the specific band response in that water type. Fig. 2A shows the spectral variability of nLw for various regions of interest (ROI; 25×25 pixel mean and standard deviation), from coastal to open ocean blue water, illustrating the diversity of water types in coastal areas. Fig. 2B shows the corresponding spectrum of the covariance ratio, $\rho(\lambda)$. The higher the ratio, the higher the I1 band covariance with the particular M(λ) band, and the higher the weight that will be applied to the sharpening.

Using this information about the covariance of bands, the weight may now be calculated and applied to the spatial resolution ratio in a stepwise process to spatially enhance all M(λ) bands with the I1 band. The next step is to compute a variability index (ϖ), which will define how each I1 band pixel at 375-m resolution ($I1_{\text{VIIRS}}$) differs from the corresponding I1 band pixel at 750-m resolution ($I1_{\text{VIIRS}}^*$):

$$\varpi = I1_{\text{VIIRS}} - I1_{\text{VIIRS}}^* \qquad (4)$$

where

$I1_{\text{VIIRS}}$ VIIRS I1 band nLw at native resolution (375-m)
$I1_{\text{VIIRS}}^*$ VIIRS I1 band nLw at 750-m resolution (2×2 pixel average, duplicated to 375-m projection)

Each 750-m I1 Band pixel is calculated by averaging a 2×2 pixel sub-array within the I1 band, and placing four duplicated pixels (2×2 average) in the original 375-m spatial projection. The variability index, ϖ, isolates the spatial difference information contained within the I1 band, and is ultimately the value that will be independently weighted for each wavelength. The spectral weight, $\omega(\lambda)$, applied to each band is calculated as the product of the covariance ratio, $\rho(\lambda)$, and the variability index, ϖ:

$$\omega(\lambda) = \varpi \rho(\lambda). \qquad (5)$$

The spectral weight term adjusts the pixel to pixel differences of the I1 band by the covariance ratio, enabling the I1 band to essentially be reconstructed using this new weight. This re-construction is made by adding the wavelength dependent weight to the VIIRS I1 Band nLw at 750-m resolution to make a weighted I1-band, $I1_{\omega(\lambda)}$:

$$I1_{\omega(\lambda)} = \omega(\lambda) + I1_{\text{VIIRS}}^*. \qquad (6)$$
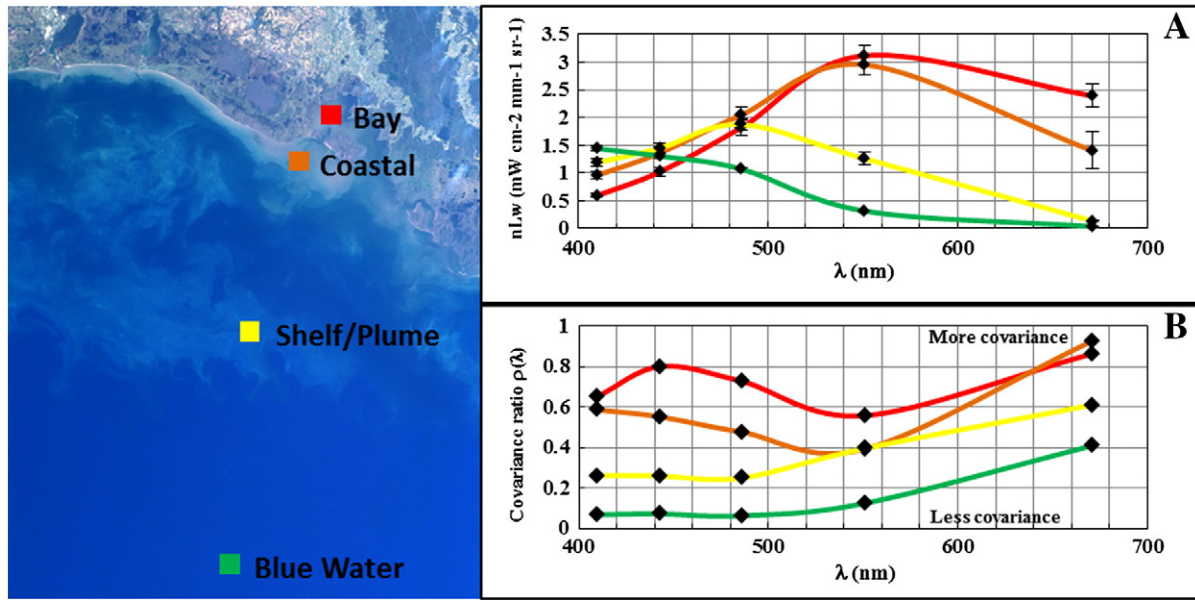
Fig. 2. Region of interest (ROI) analysis for a 25 × 25 pixel box in various water types for the northern Gulf of Mexico. The true color image (showing location of ROI) and data plots are derived from a Level 2 SNPP–VIIRS image on November 08, 2012. (A) The visible nLw spectrum for various ROI is displayed, showing different water types and (B) the corresponding visible spectrum of the covariance ratio, $\rho(\lambda)$, see Eq. (3). The amount of covariance of each M(λ) band to the I1 band will relate to how each wavelength is sharpened by the I1 band. As the amount of covariance increases/decreases, the weight of the I1 band sharpening increases/decreases proportionally.

Thus, the pixel to pixel differences existing in the weighted I1-band reflect the variance patterns of the M(λ) band being sharpened more accurately. The final step in isolating the wavelength specific variance information is to apply Eq. (1), and calculate a wavelength dependent spatial resolution ratio, $R(\lambda)$:

$$R(\lambda) = \frac{I1_{\omega(\lambda)}}{I1_{VIIRS}{}^*}. \tag{7}$$

The VIIRS 750-m M(λ) band nLw product is spatially enhanced to 375-m using:

$$M_{375}(\lambda) = R(\lambda)M(\lambda)^* \tag{8}$$

where

$M(\lambda)^*$ VIIRS M band (λ) nLw product at 750-m resolution, pixels duplicated to 375-m projection

This process is repeated for the complete visible spectrum to create a sharpened 375-m nLw product for each M(λ) band.

2.3. Derivation of bio-optical products

After obtaining a high resolution spectrum, the sharpened nLw values are placed back into the satellite processing software. The high resolution nLw products are then fed into various bio-optical algorithms to derive any existing satellite products at 375-m spatial resolution. For this study, we produced and examined the effect of increased resolution on satellite products of spectral nLw, chlorophyll-a (chl_oc3, O'Reilly, et al., 2000), and quasi-analytical algorithm (QAA) bio-optical products of absorption and backscattering (Lee, Carder, & Arnone, 2002), as well as derived beam attenuation.

We note that beam attenuation (c) cannot be directly measured by satellite radiometry, as it is the sum of total absorption (a_T) and total scattering (b) in all directions, while the satellite-detected reflectance of sunlight is only a function of total absorption and backscattering

(b_b) towards the sensor. In order to obtain beam attenuation from a space-borne sensor, there must be an integration of the volume scattering function (VSF), which describes the angular variation of scattered light in the forward and backward direction (Mobley, 1994). This ultimately enables the relation of scattering in the backward hemisphere (b_b, as seen from space) to the total scattering (b), the latter of which is the VSF integrated over all directions. Petzold (1972) normalized several measurements of VSF to total b, to obtain volume phase functions for seawater (which can be used to derive b_b from b, or vice versa), and the average of his measurements are widely used in radiative transfer equations. Operating on the principle that $c = a_T + b$, we computed beam attenuation for VIIRS using a_T from QAA (Lee et al., 2002), and converted b_b (QAA) to b using Petzold's average phase function. The average Petzold derived $b_b/b = 0.0183$ compared very well to the ratio derived from the in situ measurements used for comparisons in this study ($b_b/b = 0.0182$), therefore some quantitative evidence exists that the Petzold function used to derive satellite estimates of c should provide reasonable values in these turbid waters.

2.4. In situ data matchups and statistics

A database of in situ reflectance, inherent optical properties (IOPs), and chlorophyll fluorescence measurements were collected from three cruises spanning from August to November 2013 to validate enhanced spatial resolution products. This data encompasses a series of coastal turbid and clear water environments in the Northern Gulf of Mexico and the Chesapeake Bay (Fig. 3). A total of 44 satellite-concurrent reflectance measurements were obtained for this study, using multi-cast HyperPro data (Zibordi, D'Alimonte, & Berthon, 2004a), a modified sky-blocked floating Hyperpro (Lee, Pahlevan, Ahn, Greb, & O'Donnell, 2013), Analytical Spectral Device, Inc. (ASD) measurements following the protocols of Fargion and Mueller (2000), and data collected from the SeaPRISM AERONET site (WavCIS CSI-06, Zibordi, Mélin, Hooker, D'Alimonte, & Holben, 2004b). All reflectance data were convolved to the VIIRS relative spectral response (Moeller, McIntire, Schwarting, & Moyer, 2011). The in situ IOP data (total absorption and beam attenuation) were measured using a Wetlabs AC-9, collected from vertical profiles and a continuous
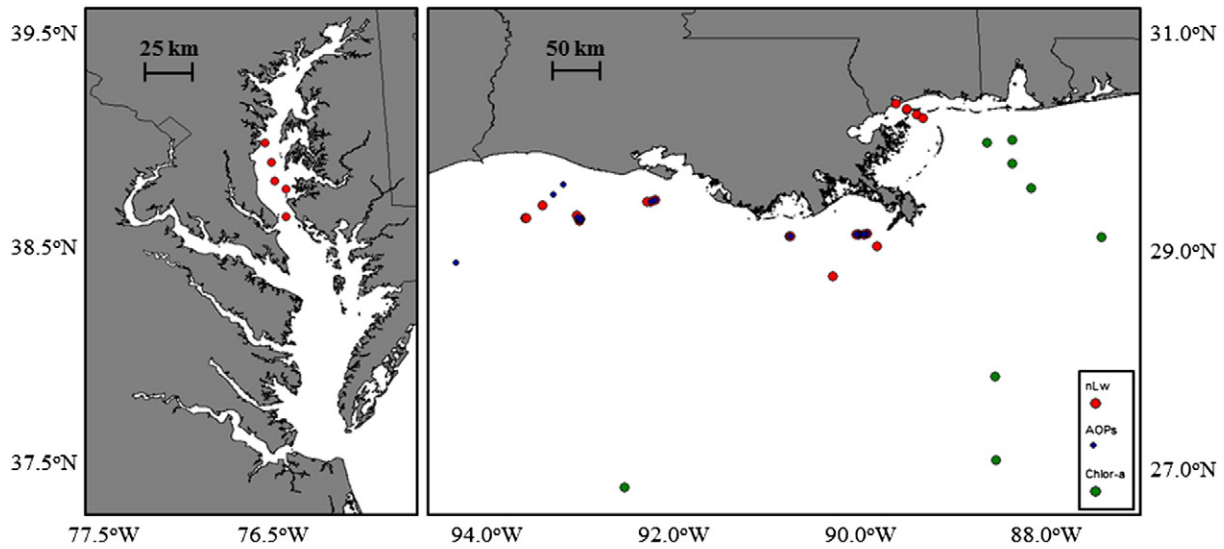
Fig. 3. Map of in situ sample locations and types used for matchup to VIIRS satellite retrievals from Chesapeake Bay, USA and the northern Gulf of Mexico, USA. Samples were retrieved from various water-types and geographic locations to provide a diverse set of measurements for algorithm assessment.

surface flow-through system equipped with a de-bubbler. Chlorophyll fluorescence data were obtained with in situ sensors (Wetlabs ECO-FL3) calibrated with fluorescence in the laboratory (Welschmeyer, 1994). Satellite and in situ matchups were within 3 h of the VIIRS over-pass, with the exception of the chlorophyll fluorescence data, where this window was opened to 5 h due to insufficient quantity of data points.

Quantitative assessments of the algorithm performance included statistical analysis to determine the functional relationships and relative errors between the in situ and satellite data. Scatter plots were generated for multiple product comparisons, including the derived regression slopes and intercepts, as well as coefficients of correlation (R). Reduced major axis (Type II) regression models were chosen over ordinary least square regression models, as all sets of measurements used in the statistical comparisons contain multiple potential sources of error (Sokal & Rohlf, 1995). We performed a Breusch-Pagan test for heteroscedasticity on all data comparisons, and removed outlier residuals until we accepted the null hypothesis of constant error variance (i.e. data was homoscedastic) to ensure validity of statistical analysis. In addition, we computed the root mean squared error (RMSE) and the normalized mean bias (NMB) between two measurements being compared, according to the following equations:

$$RMSE = \sqrt{\frac{1}{N}\sum_{i=1}^{N}(X_i - Y_i)^2} \qquad (9)$$

$$NMB = 100 * \frac{\sum_{i=1}^{N}(Y_i - X_i)}{\sum_{i=1}^{N}X_i} \qquad (10)$$

where, X is the in situ value, and Y is the satellite retrieved value. In some cases, statistics were generated to compare the relationship between two satellite-derived values, in which X is the standard VIIRS product at 750-m spatial resolution, and Y is the VIIRS product at 375-m spatial resolution. The RMSE takes into account the mean and variance of the error distribution, and defines the random error (Campbell & O'Reilly, 2006). The NMB is important as well since it defines the systemic error, and cannot be minimized with averaging.

3. Results and discussion

3.1. Algorithm output and assessment

The adaptive band sharpening technique was applied to enhance the visible nLw spectrum for a cloud-free scene in the northern Gulf of Mexico from November 08, 2012. This image covers a wide variety of water types, including a high CDOM river plume, and heavy sediment loads close to shore. Fig. 4A–E illustrates an intermediate stage of the processing, where $\rho(\lambda)$ is computed (see Eq. 3) for each wavelength. The subpanel figures illustrate where the sharpening weights are being applied at each wavelength as a function of variability relative to the I1 band. The results show that the greatest amount of sharpening (white areas) occurs at various ocean boundary regions, from coastal fronts (Fig. 4A, A-1) to offshore plumes (Fig. 4D, D-1), and varies considerably throughout the image for different wavelengths. This is because the spectral dependence of the sharpening weight varies with differing water types.

For example, even though there is less blue radiance closer to shore as a result of high CDOM absorption, the I band sharpening weight is increased at 410 nm (Fig. 4A, A-1), likely due to the presumed covariance with red backscattering (suspended particles) in close proximity to land. Fig. 4D (D-1) also shows that the 551 nm band tends to covary with the I1 band in the CDOM-rich Mississippi River plume. The ratio of red to green reflectance has been found to show a robust correlation with estimates of CDOM in coastal (Kutser, 2009; Miller, Del Castillo, & McKee, 2005; Vandermeulen, 2012) and lake (Kutser, Pierson, Kallio, Reinart, & Sobek, 2005; Menken, Brezonik, & Bauer, 2006) waters. Fig. 4E illustrates a large covariance of the 671 nm band with the 640 nm band throughout the image, which may be expected given the similar spectral characteristics between the bands. There is some deviation from this relationship into the blue offshore waters, likely due to the low signal to noise ratio of the I1 band in clear waters (Schueler et al., 2002). This showcases the self-regulating nature of the algorithm, in which large changes to radiometric quantities are moderated by reducing the weight of the denominator (I1 band) as variance between the two bands is increased. For instance, a 10-fold decrease in M(λ) band variance relative to the I1 band variance would lead to 1/10 of the original I-1 band weight to be applied, and the original M(λ) band value is not changed substantially.

From a satellite perspective, water leaving radiance is the integration of signal over the first optical depth (Gordon & McCluney, 1975).
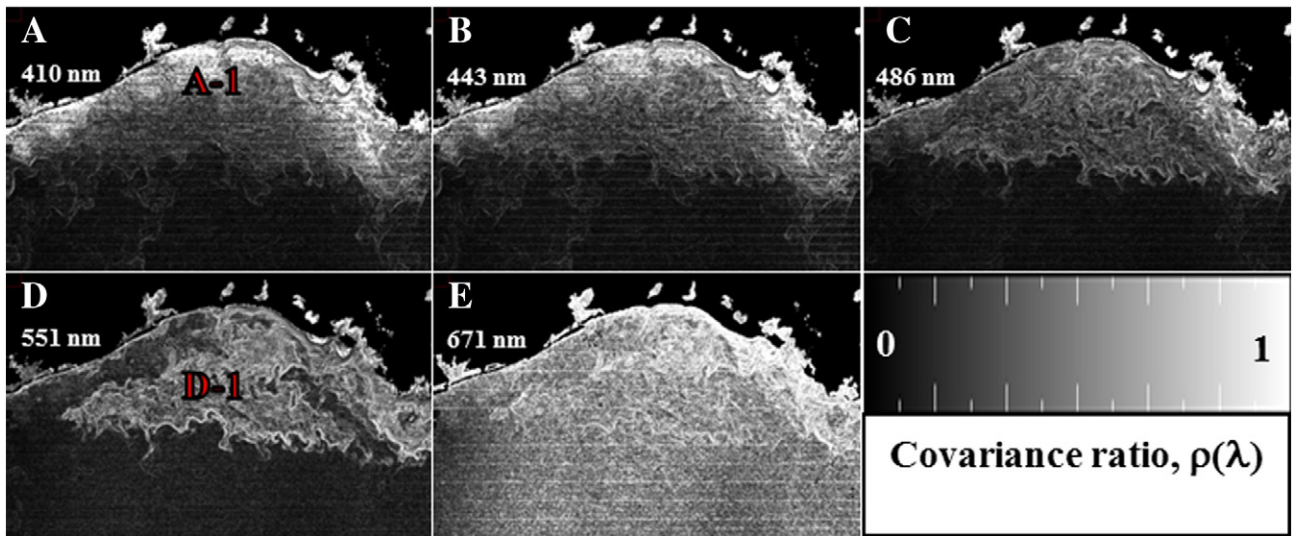
Fig. 4. Images of the λ-dependent covariance ratio, $\rho(\lambda)$ (see Eq. 2) at (A) 410 nm, (B) 443 nm, (C) 486 nm, (D) 551 nm and (E), 671 nm, an intermediate step in the adaptive sharpening technique. The lighter regions show the areas where the I1 band weight was applied higher relative to the darker regions. Notice that the weight is applied heavier within the offshore plume boundary region for the M4-band (D-1) while the coastal regions are weighted heavier in the M1-band (A-1).
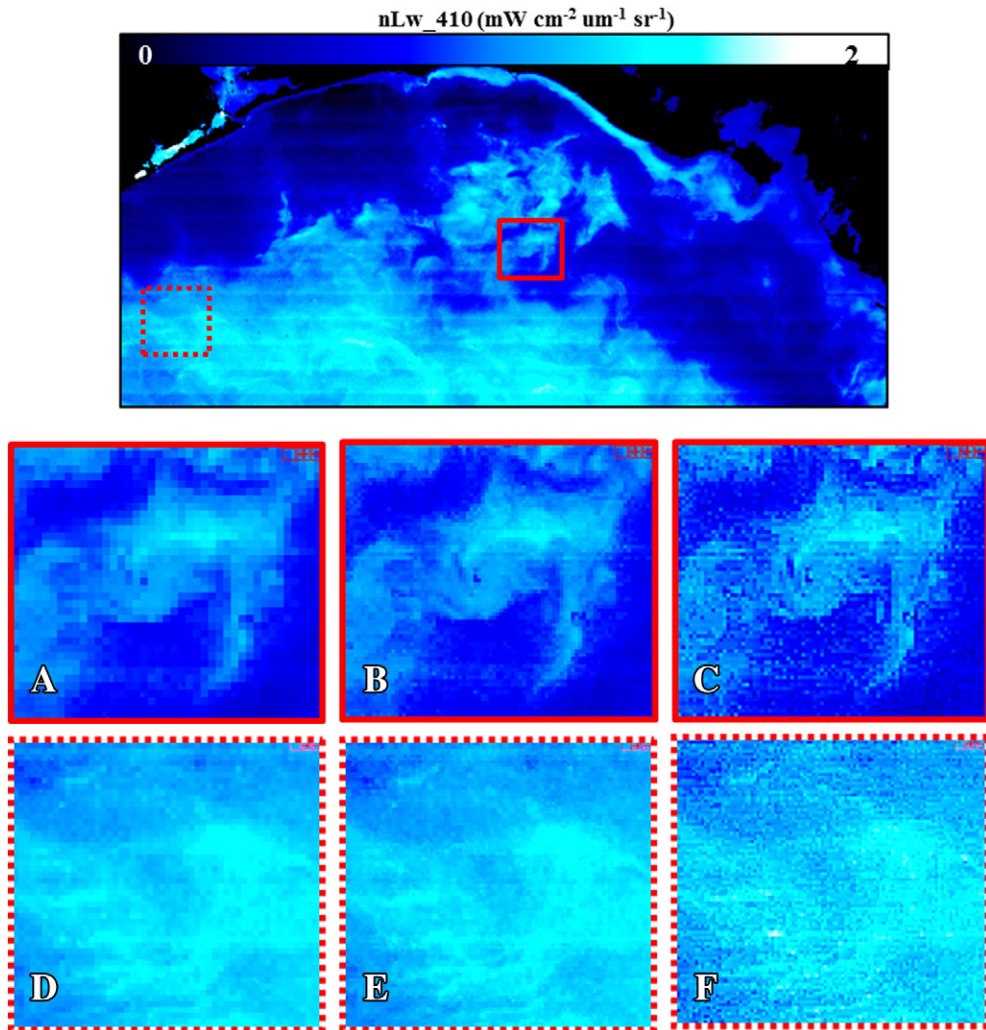

Fig. 5. Comparison of SNPP–VIIRS nLw_410 product at standard 750-m resolution (A, D), 375-m resolution with using the weighted ratio sharpening technique proposed in this paper (B, E), and 375-m resolution using a non-weighted I1 band spatial resolution ratio (C, F). A marked increase in detail in coastal gradients and optical fronts is shown in the 375-m resolution image produced from the weighted ratio (B), helping resolve ocean features in highly dynamic regions. The speckled imagery produced from the non-weighted I1 band ratio technique (C, F) illustrates the importance of correcting for spectral covariance when sharpening. Note that in the offshore blue waters (D–F), the weighted ratio (E) is not substantially different from the original 750-m resolution image (D), as the I1 band variance increases relative to the M1 band.

Therefore, changes in radiance detected from satellite imagery are dependent on subsurface optical layers, and a single M(λ) band pixel value is not necessarily the arithmetic mean of the sub-pixel variation present in spatially inhomogeneous waters with varying integration depths. While water relatively high in backscattering constituents may tend to exhibit radiance in a more 2-dimensional (horizontal) domain as light is quickly reflected from the surface of the ocean, waters dominated by penetrating absorption properties are generally 3-dimensional (horizontal and vertical) from a water leaving radiance perspective (Lee, Hu, Arnone, & Liu, 2012). Since red light from the I1 band is attenuated much more quickly than blue light, and since blue light is more affected by absorption in coastal waters, it becomes necessary to account for the difference in sub-pixel variation when using the high resolution red band to sharpen a lower resolution blue band. The sharpening methodology attempts to partially mitigate this incoherence by assuming that the changes in spatial variance between multiple bands incorporate this non-linearity of signal. For example, in a vertically stratified water mass, where the blue (M1 band) nLw signal may extend below the mixed layer, and the red (I1 band) nLw signal does not, the potentially large discontinuities in the integration depth for the two different bands would likely lead to a divergence of variance. Thus, the sharpened M1 band will only incorporate a small weighted fraction of I1 band variability, and the M1 band largely retains the larger depth-integrated radiance signal. Next, we will evaluate the viability of these assumptions made by the algorithm by examining how the subtle changes to radiometric values manifest in the imagery.

3.2. Qualitative analysis (image comparisons)

We qualitatively examined the spectrally sharpened nLw products produced for the same cloud-free scene in the northern Gulf of Mexico. Fig. 5 emphasizes the enhancement of a coastal frontal feature (Fig. 5A–C) as well as offshore blue waters (Fig. 5D–F) in the nLw 410 nm band. The nLw_410 product is chosen for display, as it is the furthermost spectral distance from the high resolution nLw_640 product, and is therefore most likely to showcase any potential artifacts introduced through the spectral sharpening process. Fig. 5A and D shows the highlighted nLw_410 features at 750-m resolution, while Fig. 5B and E shows these features at 375-m resolution, using the proposed weighted ratio technique. Figs. 5C and F also shows nLw_410 at 375-m resolution, but demonstrates some of the artifacts (speckled imagery) that are introduced into the sharpening technique when assuming that spatial variability is constant across the visible spectrum (i.e. using a single I band spatial resolution ratio for the entire spectrum). This illustrates the importance of adjusting the weight of the spatial resolution ratio according to the amount of covariance between the bands. In the offshore waters, where divergence in variability between the I1 band and the M1 band is likely to occur (Fig. 4A), there are only small differences present between the M1 band at 750-m (Fig. 5D) and the weighted M1 band at 375-m (Fig. 5E). This demonstrates that in waters where there is less confidence to utilize the I1 band variance information, the image largely remains unchanged. If the sharpening adjustment is not weighted (Fig. 5F), the I1 band variance interferes
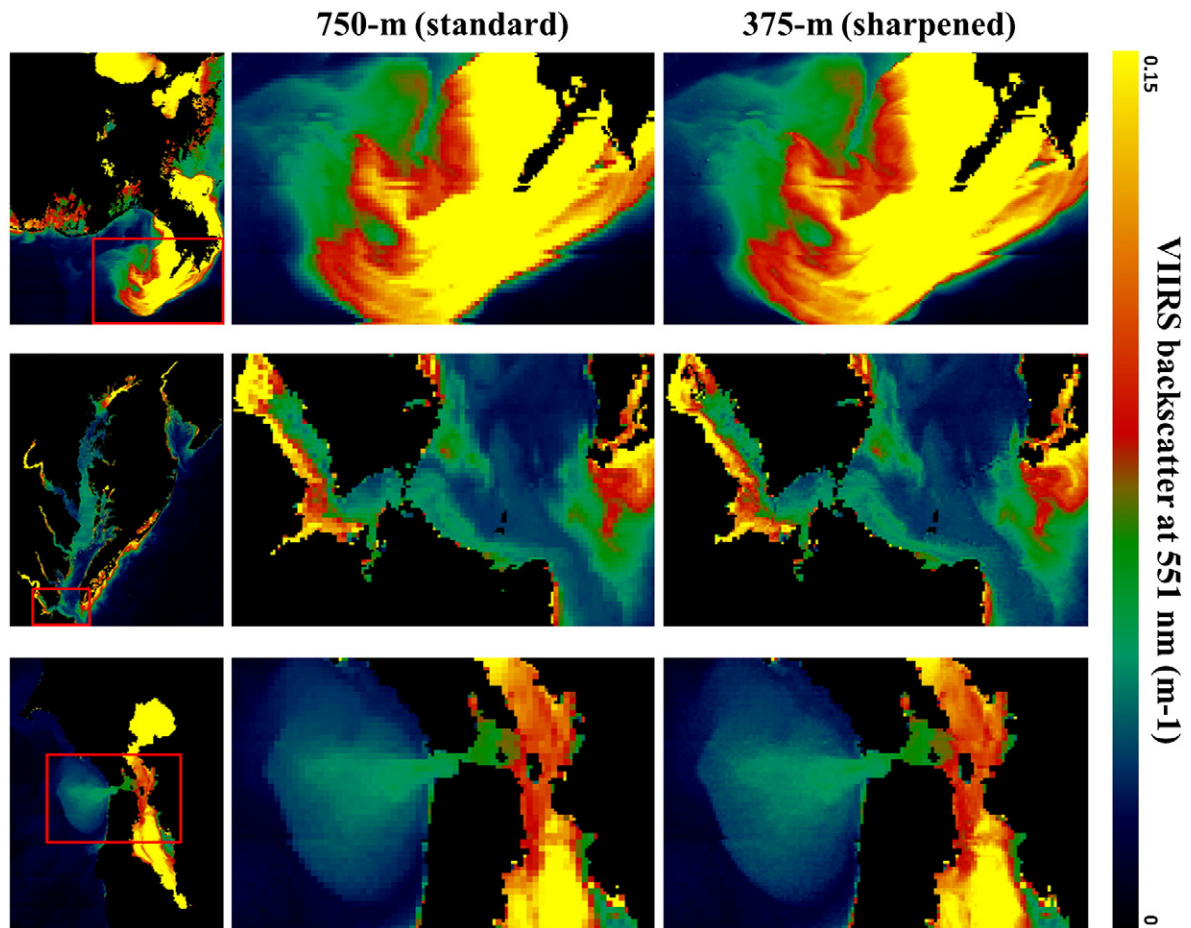

Fig. 6. Multi-regional comparison of SNPP–VIIRS backscattering at 551 nm (bb_551_qaa) product at standard 750-m resolution and 375-m resolution with using the weighted ratio sharpening technique proposed in this paper. Small errors in the spectral sharpening technique have the potential to be propagated and enhanced when pushed through the QAA. The absence of any visual irregularities and the qualitative improvement of frontal features demonstrate the advantages to band-sharpening in coastal and inland waters. Images shown: (top) Mississippi River Plume on May 14, 2013, (middle) Chesapeake Bay on April 06, 2013, and (bottom) San Francisco Bay on January 16, 2013.
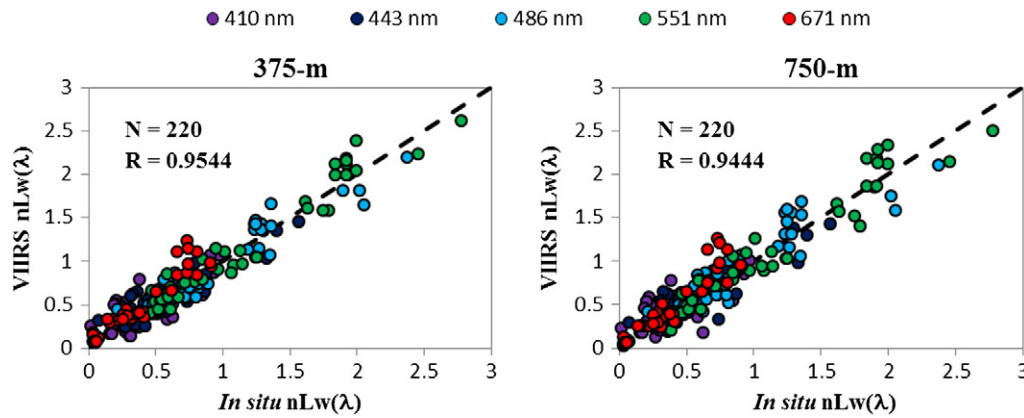
Fig. 7. Scatter plot of normalized water leaving radiance (in mW/cm^2/m/sr), comparing 220 in situ data points in various water types to the corresponding single pixel VIIRS extraction at 375-m resolution (left) and 750-m resolution (right). Note that no major outliers are introduced by the VIIRS 375-m series, suggesting that the VIIRS data is not adversely impacted by the weighted sharpening technique.

with the M1 band substantially. The quantitative spectral consistency (i.e. the preservation of the spectral shape) using the weighted sharpening technique is demonstrated by the low NMB derived from directly comparing spectral nLw values from VIIRS^{375m} and VIIRS^{750m} for a large coastal region of interest ($N = 95,160$) in the image (no plot shown; NMB = $-3.42E-03$, $-1.26E-02$, $-1.18E-02$, $-4.68E-03$, and $-7.41E-03$% for bands M1–M5, respectively).

The sharpened visible spectrum can then be used to produce high resolution bio-optical products. Fig. 6 shows the QAA backscattering product at 551 nm (bb_551_qaa) at 750-m and 375-m resolution in the Gulf of Mexico, Chesapeake Bay, and San Francisco Bay, emphasizing several turbid coastal plumes and bays. Visually, the enhancement of frontal boundaries in coastal waters demonstrates the advantage of using the proposed sharpening technique in waters where these features are prevalent. In the Chesapeake Bay image, there is even some detection of various land boundaries (e.g. bridges) that were smoothed over in the 750-m image. Fig. 6 qualitatively shows that the process of using the high resolution spectrum as input into multi-spectral algorithms does not introduce any visual artifacts into the imagery. Quantitatively, we demonstrate this low error by comparing backscattering values from VIIRS^{375m} and VIIRS^{750m} for a large region of interest in the Mississippi River outflow ($N = 95,160$), which show a low RMSE ($1.99E-03$ m^{-1}) and NMB ($1.34E-02$%). The band sharpening technique reveals a clear improvement to feature detection, and shows that there are no apparent visual irregularities introduced by the algorithm. Next, we gauge how well this enhancement of imagery will improve the estimation of in situ returns, and assess whether it provides a practical use to ocean color research.

3.3. Quantitative analysis (in situ matchups)

The quality of the sharpening algorithm was evaluated by analyzing matchups of satellite-derived values with ground measurements of

water leaving radiance. Fig. 7 shows a scatter plot of the VIIRS^{375m} and VIIRS^{750m} center pixel nLw retrievals for all wavelengths against a diverse collection of in situ spectral matchups. The plots show an overall higher R value for the comparison between the in situ data and the VIIRS^{375m} dataset, relative to the VIIRS^{750m} dataset. As a first order approximation, this may suggest an enhanced overall performance of the sharpened satellite data to represent in situ data, but importantly demonstrates that there are no major outliers introduced through the sharpening algorithm. A spectral summary of statistics comparing in situ to satellite data is shown in Table 1, enabling a more definitive quantification of errors and overall performance. The results of the spectral matchups are similar to those found from other coastal studies with the VIIRS sensor (Arnone et al., 2012; Hlaing et al. 2013; Bowers et al., 2014; Ladner et al., 2014), showing high overall correlation coefficients ($R > 0.95$) in the M3–M5 bands, and lower R values in the M1 and M2 bands. Note, at every wavelength, the correlation coefficients are higher, and the RMSE lower, for nLw estimates derived from the VIIRS^{375m} compared to VIIRS^{750m}. The higher correlations and an overall reduction in random error for 375-m satellite retrievals suggest an improvement to VIIRS estimating spectral nLw for turbid waters. The NMB values are relatively similar between the two resolutions for bands M1–M5, with VIIRS^{375m} data showing some improvement (NMB is closer to zero) in bands M1, M2, and M4, but a slightly elevated bias in M5.

Additional analysis examines the effect of placing sharpened 375-m nLw values into the satellite processing software (n2gen) to output high resolution bio-optical products. Here, any uncertainties in the spectral shape will likely be magnified in empirical chlorophyll algorithms, which use a ratio of Rrs_551 to Rrs_486 or Rrs_443 to estimate chlorophyll concentration (O'Reilly, et al., 2000). Fig. 8A shows a comparison of center pixel extractions of VIIRS^{375m} and VIIRS^{750m} chlor_a products with triplicate-averaged (where available) in situ surface chlorophyll-a measurements collected during the 2013 NOAA National Marine Fisheries Service fall plankton survey (August 21–September 02, 2014).

Table 1
Summary of statistics comparing in situ spectral water leaving radiance matchups to the corresponding single pixel VIIRS extracted nLw product at 375-m resolution and 750-m resolution. RMSE is in units of mW/cm^2/m/sr. Note that the correlation coefficients (R) are higher for the VIIRS 375-m resolution dataset at every wavelength. All values of $p < 0.001$.

|	VIIRS 375-m sharpened					VIIRS 750-m standard				
λ	410	443	486	551	671	410	443	486	551	671
Slope	1.0197	0.9470	0.9808	1.0654	1.1154	1.0188	0.9331	0.9947	1.0588	1.2015
y-int	0.0246	0.0376	-0.0013	-0.0646	0.0311	0.0271	0.0471	0.0116	-0.0666	-0.0070
R	0.6636	0.8908	0.9492	0.9715	0.9708	0.6209	0.8678	0.9311	0.9583	0.9611
RMSE*	0.177	0.143	0.138	0.135	0.115	0.188	0.156	0.160	0.160	0.116
NMB (%)	8.09	0.93	-2.05	0.19	25.61	8.64	1.11	0.74	-0.67	17.86
N	44	44	42	40	42	44	44	42	40	42
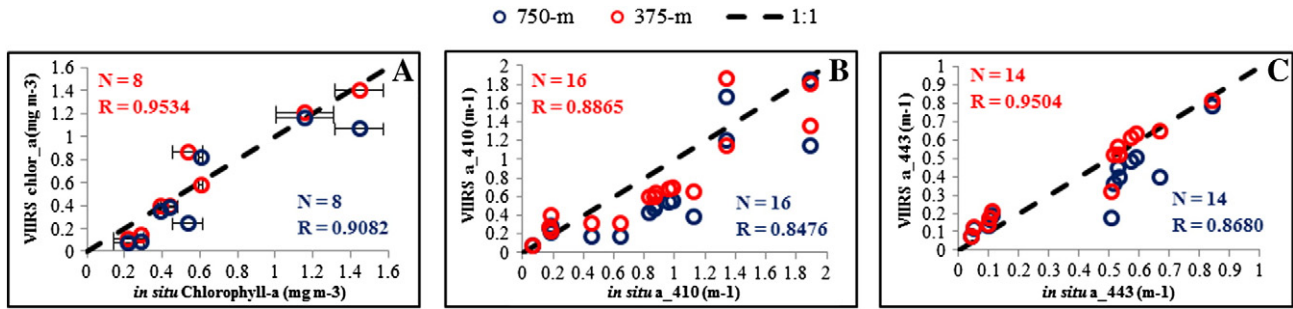
Fig. 8. Scatter plot comparisons of in situ data to corresponding VIIRS data for several bio-optical products: (A) Chlorophyll-a, (B) total absorption at 410 nm, and (C) total absorption at 443 nm. The plots show higher correlation coefficients for VIIRS at 375-m resolution data (red) to in situ absorption, compared with VIIRS at 750-m resolution (blue).

Detailed statistics of the chlorophyll-a and other bio-optical product comparisons to in situ data can be found in Table 2. This comparison demonstrates that, for this dataset, the VIIRS[375m] chlorophyll-a satellite data better represent the in situ data, as evidenced by higher correlation coefficients and lower RMSE, relative to VIIRS[750m] chlorophyll-a data. In addition, Fig. 8A shows that the VIIRS[375m] sharpening does not introduce any significant outliers when compared to in situ data, and the low NMB (Table 2) suggests that spectral shape (used as input into the chlorophyll algorithm) is not significantly altered by the use of the I1 band to optimize the sharpening scheme. Fig. 8B and C compares VIIRS[750m] and VIIRS[375m] center pixel extractions of QAA absorption products to absorption values collected during the 2013 NASA GEO-CAPE mission cruise. These comparisons have a more restrictive time window (± 3 h), and show that VIIRS[375m] offers significant enhancement of quality in matchups (higher R, lower RMSE, smaller NMB) for the critical M1 and M2 bands.

As a final assessment of the sharpening algorithm performance, the enhancement of bio-optical feature detection is evaluated. Moving beyond simply getting better matchups with ground data, we quantitatively examine if there are spatial coastal processes that can be resolved with 375-m data that are being overlooked at 750-m resolution. This requires a comparison of satellite data with a high spatial resolution optical data set. A high frequency IOP dataset was retrieved from an underway flow through system connected to a Wetlabs AC-9, courtesy of the Naval Research Laboratory's R/V Ocean Color cruise on November 20, 2013. The 32-km cruise track in the northern Gulf of Mexico crosses several notable frontal features over a three hour period, with the VIIRS overpass occurring in the middle of this time frame (Fig. 9A). Fig. 9B shows a comparison between a series of VIIRS[750m] and VIIRS[375m] single pixel extractions of the QAA total absorption (a_443_qaa) product against a continuous in situ flow through dataset (binned to 375-m) of total absorption (a_T) at 443 nm. The results demonstrate that, close to the satellite overpass (Fig. 9, b-1, b-2), the relative changes in total absorption from the in situ data set are more accurately represented by the VIIRS[375m] dataset than the VIIRS[750m] dataset. In this case, small spatial variability detected by the in situ dataset and the VIIRS[375m]

dataset are not well-defined by VIIRS[750m], presumably because the spatial binning of a 750-m pixel averages over the sub-pixel variability present (Lee et al., 2012).

Since there are not any large bio-optical fronts associated with absorption in this dataset, a comparison of in situ total beam attenuation (c) at 551 nm with satellite derived beam attenuation (c_551_qaa) was also examined (Fig. 9C). Fig. 9C shows a comparison between a series of VIIRS[750m] and VIIRS[375m] single pixel extractions of the QAA beam attenuation (c_551_qaa) product against the continuous in situ flow through dataset (binned to 375-m) of beam attenuation (c). The figure demonstrates that many strong bio-optical fronts (Fig. 9, c-1, c-2, c-3, c-4) are better resolved with the VIIRS[375m] dataset. Note that the in situ data on either end of the plot (8 km and 40 km) represents a time lag of 1.5 h from when the satellite data was collected, and shows a slight misalignment of the satellite estimated frontal features. As has been shown previously by Rantajärvi, Olsonen, Hällfors, Leppänen, and Raateoja (1998), and is re-iterated by this figure, it is extremely important to closely align the temporal scales of collected data with that of the satellite measurements, especially in dynamic coastal waters. These combined datasets clearly demonstrate that higher spatial resolution data enhance satellite returns of ocean color in coastal regions.

3.4. Implications for satellite remote sensing

The investigation into improving satellite returns for dynamic water masses brings to light the challenges associated with validation of ocean color products in coastal regions. In these waters, spatial variability, rapid temporal changes, and sampling methodology on the ground can potentially introduce as much uncertainty to a measurement as that from satellite calibration, atmospheric correction, or geophysical algorithm errors. Hence, it is useful to improve the monitoring capabilities of ocean color sensors by enhancing the spatial and temporal scales of observation, where possible. Near-term planning for the future launch of operational ocean color sensing systems in currently underway, including the design specifications for the NASA PACE (Pre-Aerosol, Clouds, and ocean Ecosystem) mission, NASA Geostationary Coastal and Air Pollution Events (GEO-CAPE) mission, ESA Sentinel 3 mission, and the NOAA Joint Polar-orbiting Satellite System (JPSS-1) mission. The development of semi-analytical algorithms that enable the exploitation of a single band to enhance the ocean color spectrum may enable a cost-effective implementation procedure to improve future monitoring from space.

4. Summary

A semi-analytical procedure for the spatial enhancement of ocean color products in optically complex waters was demonstrated for the SNPP–VIIRS sensor, providing improved products for resolving coastal dynamics. This spatial enhancement algorithm utilized the 375-m spatial resolution VIIRS I1 band (640 nm) to sharpen the 750-m M(λ)

Table 2
Summary of statistics comparing in situ derived bio-optical products (chlorophyll-a, total absorption at 410 and 443 nm) to the corresponding single pixel VIIRS extracted nLw product at 375-m resolution and 750-m resolution. RMSE is in units of mg/m³ for chlorophyll-a and m⁻¹ for QAA absorption products. All values of $p < 0.001$.

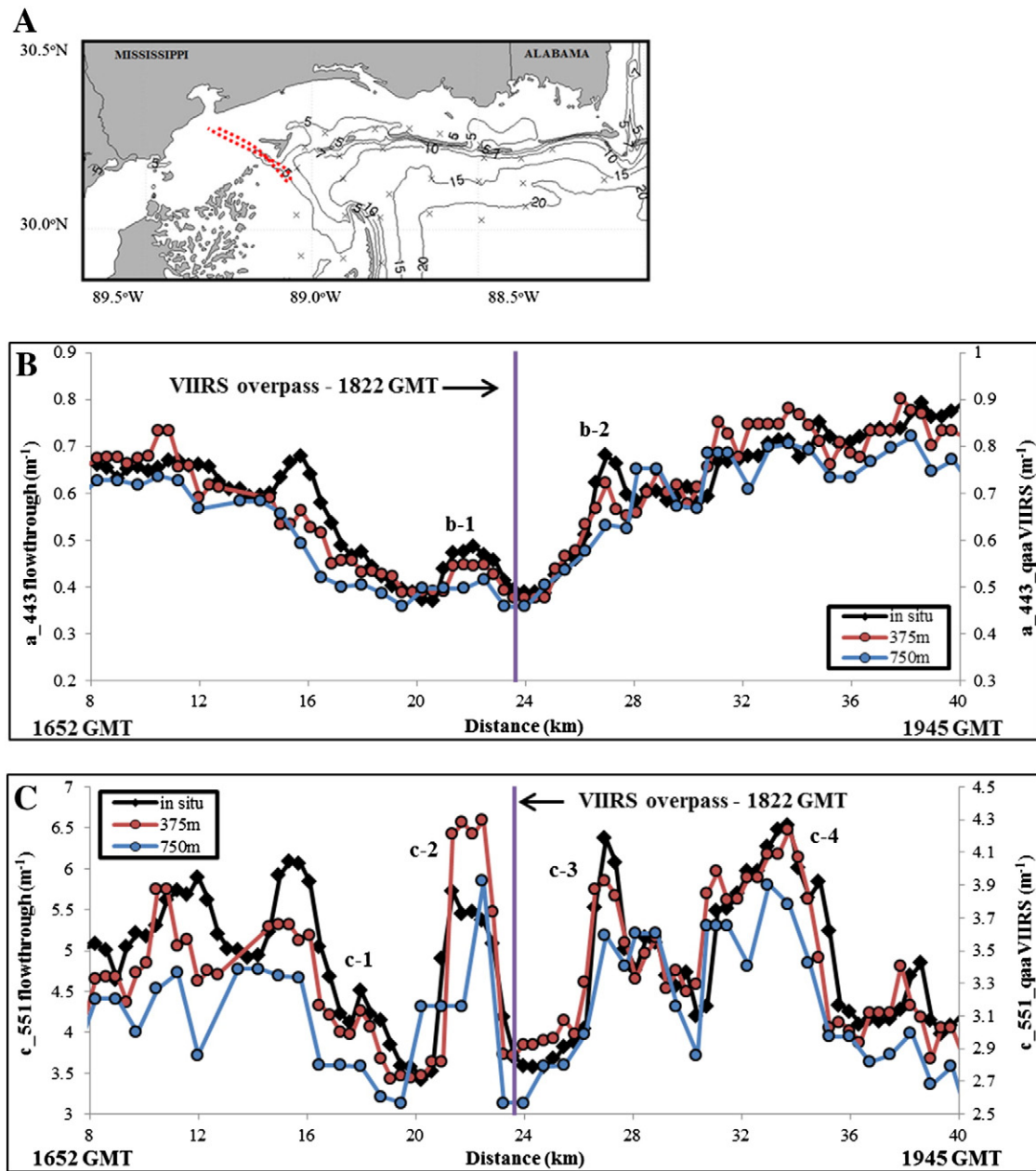|	VIIRS 375-m sharpened			VIIRS 750-m standard		
Product	chlor_a	a_410_qaa	a_443_qaa	chlor_a	a_410_qaa	a_443_qaa
Slope	1.0996	0.9487	1.0299	0.9967	0.9535	0.9607
y-int	−0.0638	−0.0904	0.0174	−0.1104	−0.2016	−0.0346
R	0.9534	0.8865	0.9504	0.9082	0.8476	0.8680
RMSE*	0.137	0.291	0.094	0.207	0.385	0.150
MNB (%)	−0.07	−15.59	7.05	−17.69	−27.99	−12.00
N	8	16	14	8	16	14

Fig. 9. An in situ flow through dataset of IOPs binned to 375-m and compared to VIIRS-derived IOPs at 375-m and 750-m resolution. The map (A) shows the location of the cruise track corresponding to the plots, below showing that the VIIRS 375-m absorption at 443 nm (B) and beam attenuation at 551 nm (C) dataset more accurately characterizes the coastal waters and frontal features than the VIIRS 750-m dataset.

bands. This approach expanded on previous work by Gumley et al. (2010) to provide atmospherically corrected normalized water leaving radiance products by spectrally weighting the sharpening algorithm as a function of the spatial covariance of the VIIRS bands. By spatially mapping where covariance exists between each M(λ) band relative to the I1 band, we proportionally adjusted the weight of the I1 band sharpening more/less in order to optimally refine the derived sub-pixel variability of the M(λ) bands. This weighting function was applied in order to account for the spectral dependence of bio-optical variability in natural systems. This novel approach was designed to reduce spectral artifacts and prevent the over-extension of the I1 band spatial information where there is less confidence to do so, such as offshore waters where the signal to noise ratio of the I1 band is diminished, or where there is a disparity in the absorption and/or scattering signal across the spectrum with varying water types.

The results described here demonstrate that the sharpened VIIRS 375-m dataset 1) did not express sensitivity to band ratio or semi-analytical algorithms, and 2) significantly increased the quality of returns for the full nLw spectrum and derived geophysical parameters (chlorophyll-a, QAA products) in comparison to the 750-m dataset. The study of dynamic coastal processes can benefit from higher spatial resolution monitoring, as suggested by the large improvements to satellite feature detection that were quantified and validated with a flow through IOP dataset. Utilizing higher spatial resolution products can also reduce uncertainties when comparing satellite data to in situ measurements, especially in coastal regions where the scales of variability are often smaller than the pixel size of many satellite sensors. The benefit of a semi-analytical approach to band sharpening is that is can potentially be applied to other satellite sensors that have wide bandwidth, high spatial resolution bands.

Acknowledgments

References

Arnone, R., Fargion, G., Martinolich, P., Ladner, S., Lawson, A., Bowers, J., Ondrusek, M., Zibordi, G., Lee, Z., Trees, C., Davis, C., & Ahmed, S. (2012). Validation of the VIIRS ocean color. Proceedings of SPIE, 8372, 83720G1–83720G10.

Arnone, R.A., Ladner, S., Fargion, G., Martinolich, P., Vandermeulen, R., Bowers, J., & Lawson, A. (2013). Monitoring bio-optical processes using NPP-VIIRS and MODIS-Aqua ocean color products. SNPP–VIIRS sensor. Proceedings of SPIE, 8724Q9, 87240Q1–87240Q9.

Aurin, D., Mannino, A., & Franz, B. (2013). Spatially resolving ocean color and sediment dispersion in river plumes, coastal systems, and continental shelf waters. Remote Sensing of Environment, 137, 212–225.

Baker, N. (2011). Joint polar satellite system (JPPS) VIIRS geolocation algorithm theoretical basis document (ATBD).

Bissett, W.P., Arnone, R.A., Davis, C.O., Dickey, T.D., Dye, D., Kohler, D., & Gould, R.W., Jr. (2004). From meters to kilometers: A look at ocean-color scales of variability, spatial coherence, and the need for fine-scale remote sensing in coastal ocean optics. Oceanography, 17, 33–43.

Bowers, J., Arnone, R., Ladner, S., Fargion, G.S., Lawson, A., Martinolich, P., & Vandermeulen, R. (2014). Regional vicarious gain adjustment for coastal VIIRS products. Proceedings of SPIE, 9111.

Campbell, J.W., & O'Reilly, J.E. (2006). Metrics for quantifying the uncertainty in a chlorophyll algorithm: Explicit equations and examples using the OC4. v4 algorithm and NOMAD data. Ocean color bio-optical algorithm mini workshop. Vol. 4. (pp. 1–15).

Davis, C.O., Kavanaugh, M., Letelier, R., Bissett, W.P., & Kohler, D. (2007). Spatial and spectral resolution considerations for imaging coastal waters. Proceedings of SPIE, 6680, 66800P1–66800P12.

Dickey, T.D. (1991). The emergence of concurrent high-resolution physical and bio-optical measurements in the upper ocean and their applications. Reviews of Geophysics, 29(3), 383–413.

Fargion, G.S., & Mueller, J.L. (2000). Ocean optics protocols for satellite ocean color sensor validation, revision 2. National Aeronautics and Space Administration, Goddard Space Flight Center.

Floricioiu, D., Rott, H., Rott, E., Dokulil, M., & Defrancesco, C. (2004). Retrieval of limnological parameters of perialpine lakes by means of MERIS data. Limnology, 16(09), 44.

Giardino, C., Candiani, G., & Zilioli, E. (2005). Detecting chlorophyll-a in Lake Garda using TOA MERIS radiances. Photogrammetric Engineering & Remote Sensing, 71(9), 1045–1051.

Gordon, H.R., & Clark, D.K. (1981). Clear water radiances for atmospheric correction of coastal zone color scanner imagery. Applied Optics, 20(24), 4175–4180.

Gordon, H.R., & McCluney, W.R. (1975). Estimation of the depth of sunlight penetration in the sea for remote sensing. Applied Optics, 14(2), 413–416.

Gordon, H.R., & Wang, M. (1994). Retrieval of water-leaving radiance and aerosol optical thickness over the oceans with SeaWiFs — A preliminary algorithm. Applied Optics, 33, 443–452.

Gumley, L., Descloitres, J., & Schmaltz, J. (2010). Creating reprojected true color MODIS images: A tutorial. (ftp://ftp.ssec.wisc.edu/pub/IMAPP/MODIS/TrueColor/).

Hlaing, S., Harmel, T., Gilerson, A., Foster, R., Weidemann, A., Arnone, R., Wang, M., & Ahmed, S. (2013). Evaluation of the VIIRS ocean color monitoring performance in coastal regions. Remote Sensing of Environment, 139, 398–414.

Hu, C., Chen, Z., Clayton, T.D., Swarzenski, P., Brock, J.C., & Muller-Karger, F.E. (2004a). Assessment of estuarine water-quality indicators using MODIS medium-resolution bands: Initial results from Tampa Bay, FL. Remote Sensing of Environment, 93(3), 423–441.

Hu, C., Nababan, B., Biggs, D.C., & Muller-Karger, F.E. (2004b). Variability of bio-optical properties at sampling stations and implications for remote sensing: A case study in the north-east Gulf of Mexico. International Journal of Remote Sensing, 25, 2111–2120.

IOCCG (2012). Mission requirements for future ocean-colour sensors. Report number 13. In C.R. McClain, & G. (Eds.), Reports and monographs of the International Ocean-Colour Coordinating Group.

Kirk, J.T.O. (1992). The nature and measurement of the light environment in the ocean. In P.G. Falkowski, & A.D. Woodhead (Eds.), Primary productivity and biogeochemical cycles in the sea (pp. 9–29). Plenum.

Kirk, J. T. O. (1994). Light and photosynthesis in aquatic ecosystems, Cambridge: Cambridge University Press.

Kutser, T. (2009). Passive optical remote sensing of cyanobacteria and other intense phytoplankton blooms in coastal and inland waters. International Journal of Remote Sensing, 30(17), 4401–4425.

Kutser, T., Pierson, D.C., Kallio, K.Y., Reinart, A., & Sobek, S. (2005). Mapping lake CDOM by satellite remote sensing. Remote Sensing of Environment, 94(4), 535–540.

Ladner, S.D., Arnone, R., Vandermeulen, R., Martinolich, P., Lawson, A., Bowers, J., Crout, R., Ondrusek, M., & Fargion, G. (2014). Inter-satellite comparison and evaluation of navy Suomi-NPP VIIRS and MODIS-Aqua ocean color properties. Proceedings of SPIE, 9111.

Ladner, S.D., Sandidge, J.C., Lyon, P.E., Arnone, R.A., Gould, R.W., Lee, Z.P., & Martinolich, P.M. (2007). Development of finer spatial resolution optical products from MODIS. Proceedings of SPIE, OP403.

Lee, Z.P., Carder, K.L., & Arnone, R.A. (2002). Deriving inherent optical properties from water color: A multiband quasi-analytical algorithm for optically deep waters. Applied Optics, 41, 5755–5772.

Lee, Z.P., Hu, C, Arnone, R., & Liu, Z. (2012). Impact of sub-pixel variations on ocean color remote sensing products. Optics Express, 20, 20844–20854.

Lee, Z., Pahlevan, N., Ahn, Y.H., Greb, S., & O'Donnell, D. (2013). Robust approach to directly measuring water-leaving radiance in the field. Applied Optics, 52, 1693–1701.

Lewis, M.R. (1992). Satellite ocean color observations of global biogeochemical cycles. In P.G. Falkowski, & A.D. Woodhead (Eds.), Primary productivity and biogeochemical cycles in the sea (pp. 139–153). Plenum.

Matthews, M.W. (2011). A current review of empirical procedures of remote sensing in inland and near-coastal transitional waters. International Journal of Remote Sensing, 32(21), 6855–6899.

Matthews, M.W., Bernard, S., & Winter, K. (2010). Remote sensing of cyanobacteria-dominant algal blooms and water quality parameters in Zeekoevlei, a small hypertrophic lake, using MERIS. Remote Sensing of Environment, 114(9), 2070–2087.

Menken, K., Brezonik, P.L., & Bauer, M.E. (2006). Influence of chlorophyll and colored dissolved organic matter (CDOM) on lake reflectance spectra: Implications for measuring lake properties by remote sensing. Lake Reservoir Management, 22, 179–190.

Miller, R.L., Del Castillo, C.E., & McKee, B.A. (2005). Remote sensing of the aquatic environment. Springer, 157–180.

Miller, R.L., & McKee, B.A. (2004). Using MODIS Terra 250 m imagery to map concentrations of total suspended matter in coastal waters. Remote Sensing of Environment, 93, 259–266.

Miller, R.L., Twardowski, M., Moore, C., & Casagrande, C. (2003). The dolphin technology to support remote sensing bio-optical algorithm development and applications. Backscatter, Alliance for Remote Sensing, 8–12.

Mobley, C.D. (1994). Light and water: Radiative transfer in natural waters. Academic Press.

Moeller, C., McIntire, J., Schwarting, T., & Moyer, D. (2011). VIIRS F1 best relative spectral response characterization by the government team. Proceedings of SPIE, 8153, 81530K.

Moses, W.J., Gitelson, A.A., Berdnikov, S., & Povazhnyy, V. (2009). Satellite estimation of chlorophyll-concentration using the red and NIR bands of MERIS—The Azov sea case study. IEEE Geoscience and Remote Sensing Letters, 6(4), 845–849.

O'Reilly, J.E., Maritorena, S., Siegel, D.A., O'Brien, M.C., Toole, D., Mitchell, B.G., Kahru, M., Chavez, F.P., Strutton, P., Cota, G.F., Hooker, S.B., McClain, C.R., Carder, K.L., Muller-Karger, F., Harding, L., Magnuson, A., Phinney, D., Moore, G.F., Aiken, J., Arrigo, K.R., Letelier, R., & Culver, M. (2000). Ocean color chlorophyll algorithms for SeaWiFS, OC2, and OC4: Version 4. In S.B. Hooker, & E.R. Firestone (Eds.), SeaWiFS postlaunch calibration and validation analyses, part 3, NASA technical memorandum.

Petzold, T.J. (1972). Volume scattering functions for selected ocean waters. Tech report no. SIO-REF-72-78. Scripps Institution of Oceanography La Jolla CA Visibility Lab.

Rantajärvi, E., Olsonen, R., Hällfors, S., Leppänen, J.M., & Raateoja, M. (1998). Effect of sampling frequency on detection of natural variability in phytoplankton: Unattended high-frequency measurements on board ferries in the Baltic Sea. ICES Journal of Marine Science: Journal du Conseil, 55(4), 697–704.

Schueler, C.F., Clement, J.E., Ardanuy, P.E., Welsch, C., DeLuccia, F., & Swenson, H. (2002). NPOESS VIIRS sensor design overview. International symposium on optical science and technology (pp. 11–23).

Sokal, R.R., & Rohlf, F.J. (1995). The principles and practice of statistics in biological research. New York: WH Freeman and Co.

Stumpf, R.P., Arnone, R.A., Gould, R.W., Martinolich, P.M., & Ransibrahamanakul, V. (2003). A partially coupled ocean–atmosphere model for retrieval of water-leaving radiance from SeaWiFS in coastal waters. Algorithm updates for the fourth SeaWiFS data reprocessing. SeaWiFS Postlaunch Technical Report Series, 22.

Vandermeulen, R. (2012). Factors influencing the spatial and temporal distribution of primary productivity and community respiration in the Mississippi Coastal Estuarine Region. Thesis.

Vandermeulen, R.A., Arnone, R.A., Ladner, S.D., & Martinolich, P. (2013). Improved monitoring of bio-optical properties in coastal and inland waters using high spatial resolution channels on SNPP–VIIRS sensor. Proc. SPIE, 8724, 87240O1–87240O9.

Welschmeyer, N.A. (1994). Fluorometric analysis of chlorophyll a in the presence of chlorophyll b and phaeopigments. Limnology and Oceanography, 39, 1985–1992.

Zibordi, G., D'Alimonte, D., & Berthon, J.F. (2004a). An evaluation of depth resolution requirements for optical profiling in coastal waters. Journal of Atmospheric and Oceanic Technology, 21(7), 1059–1073.

Zibordi, G., Mélin, F., Hooker, S.B., D'Alimonte, D., & Holben, B. (2004b). An autonomous above-water system for the validation of ocean color radiance data. IEEE Transactions on Geoscience and Remote Sensing, 42(2), 401–415.